7th International Symposium on High-Temperature Metallurgical Processing
Edited by: Jiann-Yang Hwang, Tao Jiang, P. Chris Pistorius, Gerardo R.F. Alvear F., Onuralp Yücel, Liyuan Cai, Baojun Zhao, Dean Gregurek, and Varadarajan Seshadri
TMS (The Minerals, Metals & Materials Society), 2016

EFFECTS OF MINERAL OXIDES ON THE PRECIPITATION MICRO-MORPHOLOGY OF METALLIC IRON IN THE REDUCTION OF IRON OXIDES UNDER CO ATMOSPHERE

Zhancheng GUO*, ZhiLong ZHAO, Huiqing TANG, Jingtao GAO, Lin Lin

State Key Laboratory of Advanced Metallurgy, University of Science and Technology Beijing; 30 Xueyuan Road, Haidian District; Beijing, 100083, China

Keywords: Ironmaking, Gas reduction, *In situ* observation, Iron whisker, Mineral oxides

Abstract

Grain sticking often occurs in the fluidized bed reduction of fine iron ore, which is closely related to the precipitation morphology of metallic iron on the surface of ore particles. In this work, simulating the gas-solid reduction process of iron ore, in situ observations were carried out to investigate effects of doping mineral oxides on the precipitation morphology evolution of metallic iron during reduction of iron oxides with CO. Results indicate that the precipitation morphology of metallic iron is related to the quantity of doped mineral oxides. The minimum mole fraction of doped oxide ($N_{A_yO_x}$) that can inhibit the growth of iron whiskers is related to its cation radius ($r_{A^{x+}}$), extranuclear electronic layers ($n_{A^{x+}}$) and valence electrons ($q_{A^{x+}}$). Their relation can be expressed as: $N_{A_yO_x} = 1.3\times10^{-5}\cdot\frac{r_{A^{x+}}^2\cdot\sqrt{n_{A^{x+}}}}{(q_{A^{x+}}-1)!}$

Introduction

Gas fluidized bed reduction process of fine iron ore can greatly boost the productivity due to better reduction kinetics. However, the appearance of sticking in gas-based ironmaking process results in fluidization stagnation and could spread out over the entire fluidized bed during a very short time, making it a serious problem in the fluidized bed ironmaking process[1, 2]. Numerous studies indicated that grain sticking was closely related to the precipitation morphology of metallic iron during reduction [2-10]. A good deal of fibrous whiskers were formed on the surface of particles during gaseous reduction, and the intertextures of such whiskers would lead to sticking between particles of fine ore which could influence the normal reduction [2-9]. The differences in the precipitation morphology of reduced iron can be attributed mostly to different diffusion and nucleation conditions. In addition, the chemical compositions of ore particles, especially for some composite symbiotic mineral oxides, have a strong effect on the precipitation morphology of metallic iron [2, 3, 8, 10], the systematic study of which has still not been performed. Thus, investigating the effect of mineral oxides on the precipitation morphology of metallic iron is significant in the study of sticking mechanism and inhibition measure during gaseous reduction.

In this work, under conditions of 800 ℃ and volume ratio of CO:CO_2=40:10, simulating the gas-solid reaction system on the surface of iron ore particles, *in situ* observations were performed to investigate effects of doping mineral oxides (such as MgO, CaO, SrO, BaO, Al_2O_3, Li_2O, Na_2O and K_2O) on the precipitation morphology evolution of metallic iron after the reduction.

Experimental

Experimental Apparatus

In this study, experiments were performed using an in situ observation system, which mainly includes a high-temperature stage of UK Linkam TS 1500 and a stereo optical microscope of Germany Zeiss SteREO Discovery.V20. Fig.1 schematically shows this experimental apparatus. The changes of samples surface colour and morphology were used for the characterization of the reduction process and transformation of phases.

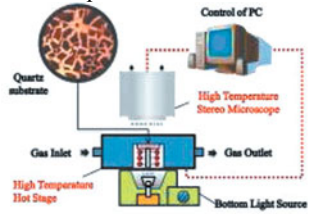

Fig.1 Experimental Apparatus of In Situ observation

Samples Preparation

Analytical reagent $Fe(NO_3)_3 \cdot 9H_2O$, $LiNO_3$, $NaNO_3$, KNO_3, $Mg(NO_3)_2 \cdot 6H_2O$, $Ca(NO_3)_2 \cdot 4H_2O$, $Sr(NO_3)_2$, $Ba(NO_3)_2$, $Al(NO_3)_3 \cdot 9H_2O$ and deionized water were used in this experiment. The mixture solutions of $Fe(NO_3)_3$ and $A(NO_3)_x$(A: Li, Na, K, Mg, Ca, Sr, Ba, Al, et al)were prepared in accordance with desired ratios. The polished quartz slide (Φ=6mm，h=1mm) was placed on refractory brick, and heated to 800℃, then cooled to about 500℃ in air. The mixture solution was then sprayed on the quartz slide. After the solution evaporated, the sample was roasted for 10min at 1000℃ to react completely and become compact. Then it was taken out and cooled to room temperature.

The principle of samples preparation was based on rapid decomposition of $Fe(NO_3)_3$ and $A(NO_3)_x$ into Fe_2O_3 and A_yO_x under high temperatures, and these oxides got deposited to the quartz slide to get the sheet sample of Fe_2O_3-A_yO_x. The reactions were:

(1) $4Fe(NO_3)_2 \cdot 9H_2O \xrightarrow{\Delta} 2Fe_2O_3 + 4NO_2\,(g) + 3O_2\,(g) + 36H_2O\,(g)$

(2) $nyA^{x+} + 2mFe^{3+} + (nxy+6m)NO_3^- \xrightarrow{\Delta} nA_yO_x \cdot mFe_2O_3 + (nxy+6m)NO_2(g) + \frac{nxy+3m-nx}{2}O_2(g)$

Fig.2 gives the characteristic of the sheet Fe_2O_3-A_yO_x: length diameter D is about 30~150 μm; short diameter d is about 10~60 μm; thickness h is about 10~50 μm.

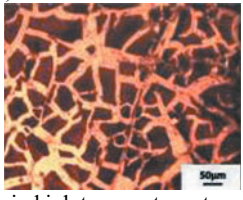

Fig.2 Images in high temperature stereo microscope

Experimental Procedure

Firstly, the quartz slide with Fe_2O_3-A_yO_x sample was placed in the high temperature hot stage, which was sealed and then put under the stereo optical microscope. The bottom of heating stage was equipped with high-brightness light source of LED. With help of these sources, the morphology variations of samples during the reduction can be observed owing to the high light transmittance for the quartz slide and sheet sample. Thus, the colour changes of sheet sample can reflect the structural evolution of iron oxides. In addition, the growth process of iron whiskers can be monitored on-line with the help of the light source from the bottom.

The heating stage was heated with the rate of 50℃/min, and kept at constant temperature after reaching the predetermined temperature (800℃), then the flow of reduction gas was kept for 30min (flow rate of CO was 40 mL/min and flow rate of CO_2 was 10 mL/min). After stopping the gas, the sample was cooled to the room temperature with the rate of 60℃/min. The whole reduction process was monitored by on-line observation under stereo optical microscope (1000x), and the images for observation were recorded at the rate of 1 sheet/s. After the above experiments, the reduced samples were subjected to SEM analysis.

Experimental Results and Discussion

In Situ Observations

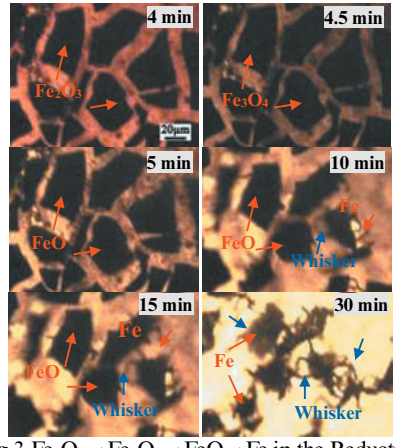

Fig.3 Fe_2O_3→Fe_3O_4→FeO→Fe in the Reduction

The precipitation morphology evolution of metallic iron after the reduction was investigated under the conditions of 800℃ and the volume ratio of CO:CO=40:10. As shown in Fig.3, results reveal that iron oxide changes from red to black at about 4 min, and the area of sheet sample expands gradually to reach to the maximum after 30 s. The area increased by 8.6% as confirmed by images analysis. Afterwards, it began to shrink, and iron whiskers started to grow. The sample colour changes during reduction was owing to the conversion of Fe_2O_3→Fe_3O_4. Fe_2O_3 is trigonal system. Moreover, Fe_3O_4 is tetragonal system. The volume could expand in this conversion. These conform to the reduction rule of iron oxide. In the conversion of Fe_3O_4→FeO, the sample colour does not change, however the volume could notably shrink. Experimental

results show that the rate for conversion of $Fe_2O_3 \rightarrow Fe_3O_4$ was very fast, which was followed by that of $Fe_3O_4 \rightarrow FeO$, but the rate for $FeO \rightarrow Fe$ was the slowest among these conversions. The whole reaction process completed in 30 min. Besides, during reduction, parts of sheet film of Fe_2O_3 tend to crack, because of the formation of Fe_3O_4 cracks in $(001)_H \| (111)_M$ with the increase of internal heat stress of the reduced sheet sample[11]. Based on observation, iron whiskers do not grow in the conversion of $Fe_2O_3 \rightarrow Fe_3O_4 \rightarrow FeO$ in the reduction of Fe_2O_3 with CO, but do in the stage of $FeO \rightarrow Fe$.

Effects of Mineral Oxides on the Precipitation Morphology

Effects of mineral oxides on the precipitation morphology of metallic iron during reduction were investigated on the basis of the reduction of Fe_2O_3 with CO. Observations for the reduction processes of all samples are shown in Fig.4 and SEM analysis after the reduction is shown in Fig.5. Concerning doping alkaline earth oxides, iron whiskers do not grow in the case of 2 mass% MgO. However, when achieving the same effect, 8 mass% CaO is needed, and the minimum quantity of doping SrO which is the same group with CaO and MgO reaches to 25 mass%. Moreover, the quantity of doping SrO reaches up to 50 mass%. Effects of the alkali metal elements on the precipitation morphology of metallic iron were further investigated. When achieving the similar inhibition, the minimum quantity of Li_2O is 0.4 mass%, however, the quantity of Na_2O is 4 mass% and the quantity of K_2O is 12 mass%. Only 0.5 mass% of Al_2O_3 which is the same period with Na_2O and MgO can totally inhibit the growth of iron whiskers.

In addition, SEM analysis (Fig.5) after the reduction shows that cracks and pores during the reduction can decrease due to doping MgO, Al_2O_3 and Li_2O into the sample. However, when doping CaO, SrO, BaO, Na_2O and K_2O, cracks and pores can increase.

Mechanism Analysis for Mineral Oxides on the Precipitation Morphology

From observations, doping mineral oxides has an obvious effect on the precipitation of metallic iron after the reduction. The samples doped with mineral oxides were analyzed by EDS. Fig.6, such as doping MgO, shows that alkaline earth elements change the distribution of Fe, and diminish the distribution density of Fe. Thus, it is conjectured that such element distribution is one of influencing factors of the growth of iron whiskers.

On the basis of experimental results, Al_2O_3, Li_2O and MgO in small quantities can effectively and totally inhibit the nucleation and growth of iron whiskers. However, for Na_2O, CaO, K_2O, SrO and BaO it needs more to achieve that effect. Thus, the precipitation morphology variation of the reduced iron is fundamentally related to the fresh structures after doping mineral oxides.

To understand the state for every element with uniform distribution, XRD was used for the reduced samples. As shown in Fig.7, the peaks shape of all samples are similar to that of Fe_2O_3 and ferrate of corresponding oxides, but simple oxides, i.e. Fe_2O_3 and A_yO_x, are not formed. Therefore, doped elements enter the Fe_2O_3 lattice to form a series of compounds such as A_yO_x-Fe_2O_3. Taking $MgFe_2O_4$ of spinel structure as an example, oxygen is closely arranged with face-centred cubic, and Mg^{2+} and Fe^{3+} are respectively filled in the framework of O^{2-}, which contains 64 tetrahedral interstitials and 32 octahedral interstitials. It is seen that doped cations fill in these tetrahedral interstitials and octahedral interstitials to form similar spinel structure, which leads to absence of iron whiskers.

In such structures with ionic species, all the oxides have great differences on inhibition for the growth of iron whiskers, which is possibly related to the character of cations of doped oxides as seen in Table.1. Because ionic compounds are formed after doping elements, considering the

coordination and electrons spinning of the cations of doped oxides and Fe, effects of all ions on the reduction were investigated by using the radius of Shannon [12] in this work.

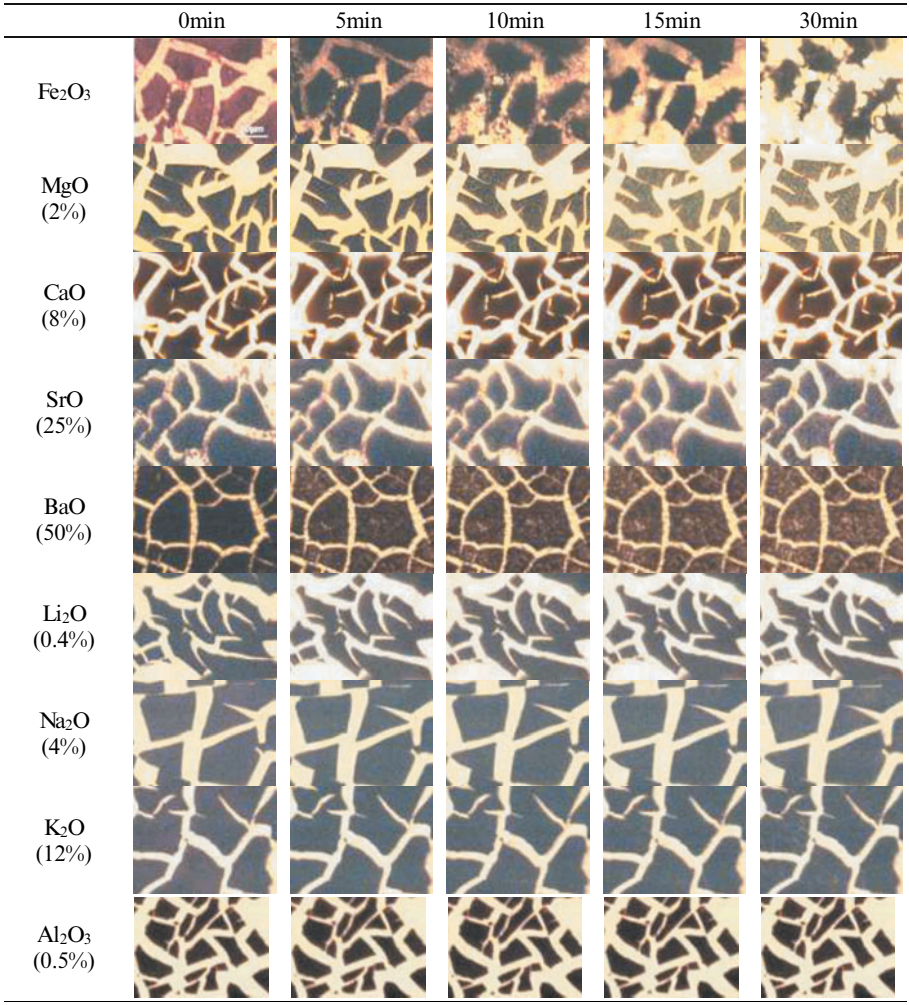

Fig.4 In situ observations for effects of mineral oxides on the reduction of iron oxides

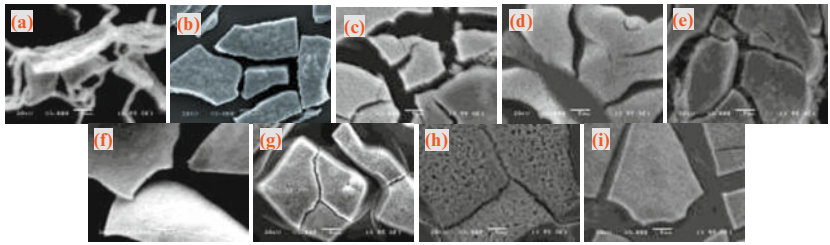

Fig.5 SEM analysis for effects of different mineral oxides on the precipitation morphology of metallic iron: (a)Fe_2O_3, (b)2%MgO, (c)8%CaO, (d)25%SrO, (e)50%BaO, (f)0.3%Li_2O, (g) 4%Na_2O, (h) 12%K_2O, (i) 0.5%Al_2O_3

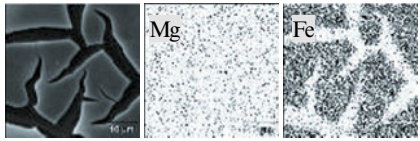

Fig.6 SEM Images for the sheet oxide iron with 2 mass% MgO and surface scanning image of elements

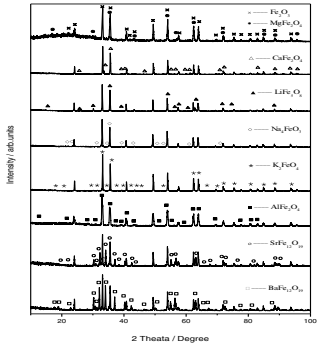

Fig.7 XRD analysis of samples after doping mineral elements with the same concentrations

Table1 Cation character of all mineral oxides

Cation (A)	Radius for Shannon(r/pm)	Extranuclear electronic layers (n/ ind)	valence electrons (q/ ind)
Mg^{2+}	65	2	2
Ca^{2+}	99	3	2
Sr^{2+}	133	4	2
Ba^{2+}	135	5	2
Li^{+}	60	1	1
Na^{+}	95	2	1
K^{+}	133	3	1
Al^{3+}	50	2	3
Fe^{2+}	76	3	2
Fe^{3+}	64	3	3

Judging from the ion characters, ions with large radius, many extranuclear electronic layers and few valence electrons have certainly few charges in the unit volume, and have a weaker adsorption for atom Fe and atom O. Therefore, only enough mineral oxides can inhibit the migration and oriented growth of Fe crystal. Furthermore, they avoid the formation and growth of iron whiskers. Thus, the minimum mole fraction of doping oxide which can inhibit the growth of iron whiskers ($N_{A_yO_x}$) is proportional to its cation radius ($r_{A^{x+}}$), and is inversely proportional to its extranuclear electronic layers ($n_{A^{x+}}$) and its valence electrons ($q_{A^{x+}}$), which can be expressed as follows:

$$F(N_{A_yO_x}) \sim \frac{f(r_{A^{x+}}) \cdot f(n_{A^{x+}})}{f(q_{A^{x+}})}$$

On the basis of observations, a relation was obtained by regression analysis for the quantities of all oxides:

$$N_{A_yO_x} = 1.3\times10^{-5} \cdot \frac{r_{A^{x+}}^2 \cdot \sqrt{n_{A^{x+}}}}{(q_{A^{x+}}-1)!} \quad (\text{r: pm})$$

Table.2 shows the comparison of observations and the predictions by equation. Results indicate that the practical quantities of doping oxides are consistent with those predicted by the equation.

Overall, the minimum quantities of doping mineral oxides, which can influence the precipitation morphology of metallic iron in the reduction Fe_2O_3 with CO, are related to their cation radius, their valence electrons and their extranuclear electronic layers. The larger the radius of doping cation is, the more extensive the [FeO_6] lattice structure is restructured and consequently, the reduction reaction will be accelerated, and the minimum quantity of doping oxide to inhibit the growth of iron whiskers will gradually increase. Conversely, the less the radius is, the less the [FeO_6] lattice structure is destroyed. Moreover, the cracks and pores are not formed in the reduction.

Therefore, to inhibit well the nucleation and growth of iron whiskers and furthermore to avoid the gain sticking, the particle surface can be treated by the modification of cations. The cation with small radius and many valence electrons should be first selected considering decreasing its quantity and cost.

Table 2 Comparison of the quantities of doping oxides for formula and experiment

Mineral oxide (A_xO_y)	Formula parameter			Quantity by formula		Quantity by exp.
	$r_{A^{x+}}$	$n_{A^{x+}}$	$q_{A^{x+}}$	$N_{A_yO_x}$	$W_{A_yO_x}$%	$W'_{A_yO_x}$%
MgO	65	2	2	0.078	2.06	~2
CaO	99	3	2	0.221	9.02	~8
SrO	113	4	2	0.332	24.42	~25
BaO	135	5	2	0.530	49.10	~50
Li_2O	60	1	1	0.047	0.45	~0.4
Na_2O	95	2	1	0.166	3.39	~4
K_2O	133	3	1	0.398	12.75	~12
Al_2O_3	50	2	3	0.023	0.74	~0.5

Conclusions

(1) Metallic iron is mostly formed as iron whisker in the reduction of iron oxides with CO under 800℃. The reduction rate in the conversion of $Fe_2O_3 \rightarrow Fe_3O_4$ is faster than that of $Fe_3O_4 \rightarrow FeO$. However, the conversion of $FeO \rightarrow Fe$ is slow and lasting. The changes of colour and volume can be attributed to the lattice transformation in the conversion of $Fe_2O_3 \rightarrow Fe_3O_4 \rightarrow FeO$, with consequent formation of cracks and pores. The nucleation and growth of iron whiskers also occur during the conversion of $FeO \rightarrow Fe$.

(2) From the effects of doping elements on the morphology of iron whiskers, MgO、Al_2O_3、Li_2O can inhibit the formation and growth of iron whiskers, respectively, and CaO and Na_2O can inhibit their nucleation and promote their growth with the increasing quantity of doping oxide. However, SrO and BaO promote nucleation and growth. In addition, MgO, Al_2O_3 and Li_2O can reduce the occurrence of cracks and pores during reduction, and on the other hand CaO, SrO, BaO, Na_2O and K_2O can contrary promote such cracks and pores.

(3) Doping mineral oxides can change the precipitation morphology of metallic iron after the reduction. The mole fraction of doping oxide ($N_{A_yO_x}$) is related to its cation radius ($r_{A^{x+}}$), its extranuclear electronic layers ($n_{A^{x+}}$) and its valence electrons ($q_{A^{x+}}$). The more the cation radius is, the less the quantity of doping oxide added. In contrast, the less the cation radius is, the more the quantity of doping oxide is. The minimum mole fraction of doping oxide can be expressed as:

$$N_{A_yO_x} = 1.3\times10^{-5} \cdot \frac{r_{A^{x+}}^2 \cdot \sqrt{n_{A^{x+}}}}{(q_{A^{x+}}-1)!}$$

Acknowledgement

This work is supported by National Natural Science Foundation of China, Project 51234001

References

1. Istitute of Chemical Metallurgy of Academia Sinica, Institute of Scientific and Technical Information of China, *Gas ironmaking in Fluidized Bed* (Beijing: Scientific and Technology Literature Publishing House, 1977).
2. Komatina M, Gudenau H W, "The Sticking problem during direct reduction of fine Iron ore in the fluidized bed," *Metalurgija*, (2004), 309-328.
3. Degel R, "Eisenerzreduktion in der Wirbelschiht mit wasserstoffreichem Gas: Sticking und Ansätze," (Dissertation, Germany, RWTH Aachen 1996).
4. Schiller M, "Mikromorphologie der Eisenphase als Folge der Reduktion von Eisenoxiden. Dissertation," (Germany, RWTH Aachen 1987).
5. Gudenau H W, Hirsch M, Denecke H, et al, "Direct reduction of iron ore fines in a fluidized bed using hydrogen-rich gas," *Stahl und Eisen (Germany)*, 117(4) (1997), 91-99.
6. Gudenau H W, Fang J, Hirata T, et al, "Fluidized bed reduction as the prestep of smelting reduction," *Steel Res*, 60(314) (1989), 138-44.
7. Fang J, "Sticking problem in fluidized bed iron ore reduction," *China: Iron Steel*, 26 (5) (1991), 11- 14.
8. Zhilong Zhao, Huiqing Tang, Zhancheng Guo, "In situ observation and mechanism research of the influence of CaO on the growth of iron whiskers under CO atmosphere," *Journal of University of Science and Technology Beijing*, 33(7) (2011), 817-22.
9. Nicolle R, Rist A, "The Mechanism of Whisker Growth in the Reduction of Wüstite," *Metallurgical Transactions B*, 10B (1979), 429-36.
10. Bartels M, Lin W G, Nijenhuis J, "Agglomeration in fluidized beds at high temperatures: Mechanisms, detection and prevention," *Progress in Energy and Combustion Science*, 34(5) (2008), 633-66.

11. Kashiwaya Y, Yamaguchi Y, Kinoshita H, et al, “In Situ Observation of Reduction Behavior of Hematite with Solid Carbon and Crystallographic Orientation between Hematite and Magnetite,” *ISIJ International*, 47(2) (2007), 226-33.
12. Shannon By R D, “Revised Effective Ionic Radii and Systematic Studies of Interatomie Distances,” *Acta Cryst*, A32 (1976), 751-67.